Lattice Oxygen Mobility and Structural Stability of Ni and Cu Octahedral Molecular Sieves Having the Cryptomelane Structure

Yuan-Gen Yin,[†] Wen-Qing Xu,[†] and Steven L. Suib*[,‡]

Department of Chemistry, Department of Chemical Engineering, and Institute of Materials Sciences, University of Connecticut, Storrs, Connecticut 06269-3060

C. L. O'Young*

Texaco Research Center, Texaco, Inc., P.O. Box 509, Beacon, New York 12508

Received August 11, 1994[⊗]

Oxygen species in Ni and Cu octahedral molecular sieves (OMS) having a 2 × 2 tunnel structure similar to that of cryptomelane or hollandite have been studied in detail through stepwise-ramping temperature-programmed reduction in CO/He, as compared to constant-ramping temperature-programmed reduction. The availability, recoverability, and structural stability of lattice oxygen in Ni-OMS-2 and Cu-OMS-2 were studied by means of monitoring the isothermal reduction and oxidation with CO/He and O_2/He, respectively, in combination with X-ray diffraction studies. Results suggest there is a much higher resolution of oxygen species with a stepwise-ramping temperature-programmed technique. Quantitation of uptake and loss of oxygen to and from the lattice shows increasing mobility with increasing temperature of reduction/oxidation. The mobility decreases with subsequent redox cycles. The structure of OMS-2 survives to a certain extent following the redox cycle but collapses more severely at higher temperature. A compromise was chosen for maximum recoverability of oxygen and for minimum damage to crystallographic structure.

Introduction

Mixed metal oxides were widely used in many fields such as catalysis[1] and electrochemistry[2] and in chemical sensors.[3] The effectiveness of metal oxides for serving as catalysts for partial or total oxidation, as electrode materials for electrochemical and electrocatalytic applications, and as solid-state chemical sensors for reductive gases are usually dominated by their capability and propensity of cycling between different valence states of relevant cations and mobility of lattice oxygen ions. These factors are determined intrinsically by the binding situation between local metal and oxygen atoms, or, in short, M−O bonding. Knowledge about the behavior of different M−O bonding in various applications would be very informative. For example, in oxidative catalysis, it is generally accepted that surface O^- or O_2^- is responsible for the total oxidation of hydrocarbons;[4] however, lattice oxygen ions are much more selective in partial oxidation reactions.[5] In view of the presence of several inequivalent M−O bonds in a mixed metal oxide, the M−O bonds have considerable variation in strength, leading to changes in catalytic selectivity. Structure−behavior relationships can also be derived for electrochemical or electrocatalytic materials and sensors. For example, it was inferred that the strength of the metal−oxygen bond in some perovskites ($LnMO_3$) is an important factor for sensing methanol.[6] The high oxygen mobility at elevated temperature of some copper perovskites suggests possible applications of these compounds as oxygen sensors.

Fierro *et al.*[8] indicated correlations between oxygen adsorption on lanthanum manganite perovskites and their reducibility, as well as the importance of studying these properties. Oxygen species with different binding strengths can be probed through the ease of the release of oxygen in temperature-programmed desorption (TPD) and the reactivity of oxygen with hydrogen or other reductants via temperature-programmed reduction (TPR). The TPD and TPR techniques have proved to be very useful for investigating oxygen species of the single and mixed metal oxides, shedding some light on the types of oxygen species and their properties, such as binding energies, populations, and reactivities. Adsorbed (or absorbed) oxygen species can usually be discerned from lattice oxygens of different binding energies by their peak positions in the TPD/TPR spectra. Whether the oxygen species exist in discrete states or with a broad distribution of binding strengths is of interest. In this respect, it seems that temperature-programmed techniques can offer higher resolution as compared to other techniques. On the one hand, the peak positions in TPD or TPR spectra are measures of stability or reactivity of oxygen species. On the other hand, the area under a peak is a measure of the availability of oxygen species in specific temperature regimes. Of course, other techniques for probing the surface and/or bulk composition, the structure, and environments around the metal center are still indispensable in helping to elucidate the identity of oxygen species and changes that occur during redox reactions.[5,9,10]

[†] Department of Chemistry, University of Connecticut.

[‡] Department of Chemistry, Department of Chemical Engineering, and Institute of Materials Sciences, University of Connecticut.

[⊗] Abstract published in *Advance ACS Abstracts,* July 1, 1995.

(1) Oyama, S. T.; Desikan, A. N.; Hightower, J. W. In *Catalytic Selective Oxidation*; Oyama, S. T., Hightower, J. W., Eds.; ACS Symposium Series No. 523; American Chemical Society: Washington, DC, 1993; p 6.

(2) Myles, K. M.; McPheeters, C. C. *J. Power Sources* **1990**, *29*, 311−319.

(3) Janata, J. *Chem. Rev.* **1990**, *90*, 691−703.

(4) Kung, H. H. *Studies in Surface Science and Catalysis: Transition Metal Oxides*; Vol. 45; Elsevier: Amsterdam, 1989; Chapter 7.

(5) Brazdil, J. F. In *Characterization of Catalytic Materials*; Wachs, I. E., Ed.; Butterworth-Heinemann: Boston, 1992; Chapter 3.

(6) Tejuca, L. G.; Fierro, J. L. G. *Adv. Catal.* **1989**, *36*, 237−328.

(7) Engler, E. M. *CHEMTECH* **1987**, *17*, 542−551.

(8) Fierro, J. L. G.; Tascón, J. M. D.; Tejuca, L. G. *J. Catal.* **1984**, *89*, 209−216.

0020-1669/95/1334-4187$09.00/0

In our previous studies of octahedral molecular sieve (OMS) materials of manganese dioxide composition, TPD/TPR techniques were used to observe several oxygen species. Some oxygen species were reactive to hydrogen or CO at successively higher temperatures and have been distinguished and related to their lattice positions.[11,12] However, in many cases, the TPD/TPR spectra show a multitude of peaks adjoined to each other to form a broad hump that is difficult to resolve. That means, even before one oxygen species is evolved during TPD or consumed in TPR at its maximum rate, the onset of evolution/consumption of subsequent oxygen species has already begun. Deconvolution of such data with SigmaPlot is not a perfect solution to this problem.[12]

In this paper, the availability of oxygen species in Cu-OMS-2 and Ni-OMS-2 materials having the 2 × 2 MnO_6 structure of cryptomelane are further delineated by new techniques: stepwise TPR in CO/He and monitored isothermal redox cycles with CO/He and O_2/He. The difficulty in discriminating adjoining TPR peaks is greatly alleviated by using a stepwise reduction technique. Monitored isothermal reduction and reoxidation, as well as oxygen pulse treatments, were then conducted at temperatures selected on the basis of results from stepwise reductions in order to study the recoverability of oxygen species and, in combination with X-ray diffraction studies, to study the retention or restorability of the OMS-2 structure.

Experimental Section

Synthesis. The doped OMS-2 samples were prepared by refluxing an aqueous suspension resulting from the reaction of potassium permanganate and manganous(II) sulfate with the addition of nitrates of the doping metals.[13] After filtering and washing, the solid samples were dried at 120 °C to avoid loss of oxygen during calcination. The surface area of Ni- and Cu-OMS-2 are 73 and 94 m^2/g, respectively. The bulk atomic ratios, determined by ICP-AES methods, are Ni:K:Mn = 0.038:0.84:8.0 for Ni-OMS-2 and Cu:K:Mn = 0.11:0.83:8.0 for Cu-OMS-2, respectively, as there are eight Mn atoms present per unit cell of cryptomelane/hollandite. The samples were purged with He at room temperature to remove loosely bound oxygen on the surface before being subjected to reduction studies.

Stepwise-Ramping Reduction Techniques. In the TPR technique, the Cu-OMS-2 and Ni-OMS-2 samples, 20.0 mg, were loaded into a 6 mm quartz reactor, and a stream of 4.90% CO/He gas was flowed at a rate of 30.0 sccm through the reactor in a tubular furnace at room temperature. After steady state was reached [as shown by a downstream thermal conductivity detector (TCD)], the OMS-2 samples were subjected to reduction at successively higher temperatures. For the constant-ramping mode, the temperature of the furnace was linearly ramped at 15 K/min from 298 to 943 K. With the stepwise-ramping mode, the furnace temperature was raised at approximately 15 K/min, with soaking at each selected temperature, for 7 min. For both modes, the consumption of CO in the gas stream was monitored by TCD after condensation of any water vapor, which was trapped in liquid N_2. Hence, oxygen loss is accounted for via oxidation of CO only from lattice oxygen.

Monitored Isothermal Reduction. In the monitored isothermal reduction, a feed of 4.90% CO/He was passed through the sample in the quartz reactor at 30.0 sccm. When the signal of a TCD which was used to monitor the change in concentration of CO in the gas stream reached a steady state condition, the reactor was quickly placed into a tubular furnace maintained at a constant specified temperature. A brief dip in the temperature of the reactor (about 1 min) is observed before the reactor resumed a steady temperature. The diminution in CO concentration due to oxidation by oxygen species in OMS-2 samples was monitored by the change in TCD signal. The reduction was concluded when the TCD signal resumed its original base line. Generally, 20 min was required.

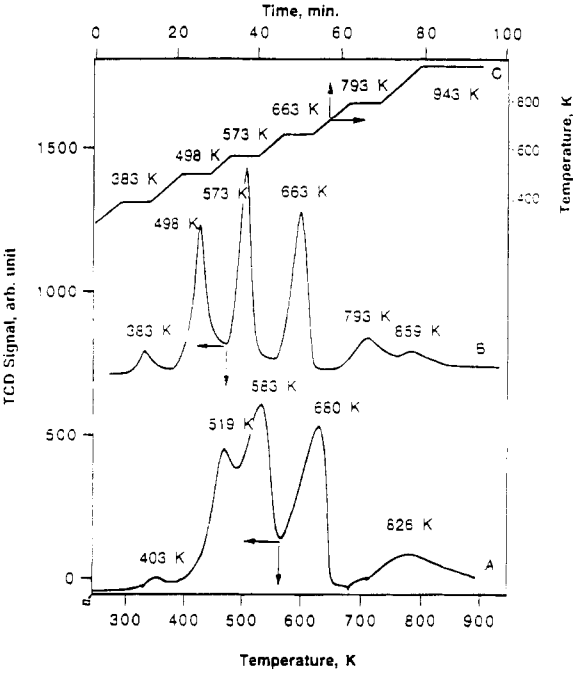

Figure 1. Stepwise- and constant-ramping TPR of Ni-OMS-2 in CO/He: (A) constant-ramping TPR; (B) Stepwise-ramping TPR; (C) temperature profile.

Oxygen Pulsing and Monitored Isothermal Oxidation. After reduction by CO/He, the reduced OMS-2 samples were reoxidized, either by oxygen pulsing or by monitored isothermal oxidation. For oxygen pulsing, a sequence of oxygen pulses (2.57 μmol in size) was passed successively over the sample in the furnace at the same temperature after reduction until the area of the oxygen pulse is close to the pulse area at room temperature. The standard oxygen pulse area was calibrated from time to time. Reproducibility (percentage of deviation from average value) is within 0.58% of the average. The diminution in pulse area was summed up, and the oxygen uptake by the reduced OMS-2 samples from all pulses was calculated. The procedures for monitored isothermal oxidations were the same as that in monitored isothermal reduction, except a stream of 4.80% O_2/He was used instead of CO/He. The change in oxygen concentration of the O_2/He stream was also monitored by TCD when the gas stream was passed through the reduced OMS at specific temperature. The TCD is extremely sensitive, and a loss of even 0.0015 μatom of oxygen species per millimole of OMS-2 sample can be detected. This is comparable to the detection limit of an electromicrobalance.

X-ray Powder Diffraction. The X-ray powder diffraction patterns of Cu-OMS-2 and Ni-OMS-2 after various treatments were collected by using a Scintag 2000 XDS diffractometer with Cu Kα X-ray radiation. A 0.02 step in 2θ/count, a beam voltage of 45 kV, and a beam current of 40 mA were used. JCPDS powder diffraction data files[14] were used as references for phase identification of cryptomelane/hollandite. The X-ray diffraction patterns of fresh and treated OMS-2 were overlaid via Quattro/Window software.

Results

Temperature-Programmed Reduction. A stepwise-ramping TPR of Ni-OMS-2 in CO/He is shown in Figure 1 together

(9) Suib, S. L. In *Photochemistry and Photophysics*; Rabek, J. F. Ed.; CRC: Boca Raton, FL, 1991; Vol. III, pp 1–40.
(10) Dixit, L.; Gerrard, H. J.; Bowley, H. J. *Appl. Spectrosc. Rev.* **1986**, *22*, 189–249.
(11) Yin, Y. G.; Xu, W. Q.; Shen, Y. F.; Suib, S. L.; O'Young, C. L. *Chem. Mater.* **1994**, *6*, 1803–1809.
(12) Yin, Y. G.; Xu, W. Q.; DeGuzman, R. D.; Suib, S. L.; O'Young, C. L. *Inorg. Chem.* **1994**, *33*, 4384–4389.
(13) DeGuzman, R. D.; Shen, Y. F.; Neth, E. J.; Suib, S. L.; O'Young, C. L.; Levine, S.; Newsam, J. M. *Chem. Mater.* **1994**, *6*, 815–821.
(14) The following JCPDS-ASTM powder diffraction data files were taken into account for phase identification of cryptomelane and hollandite: 38-476, 34-174, and 29-1020.

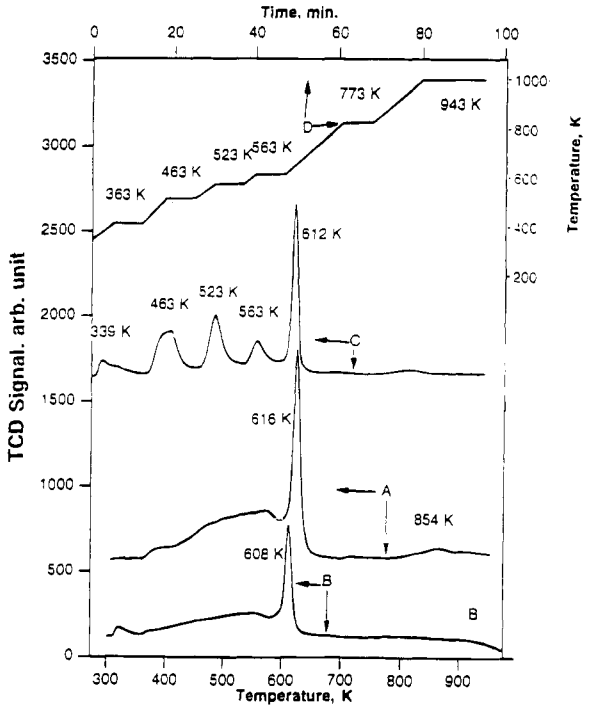

Figure 2. Stepwise- and constant-ramping TPR of Cu-OMS-2 in CO/He: (A) constant-ramping TPR (15 K/min); (B) constant-ramping TPR (5 K/min); (C) stepwise-ramping TPR; (D) temperature profile.

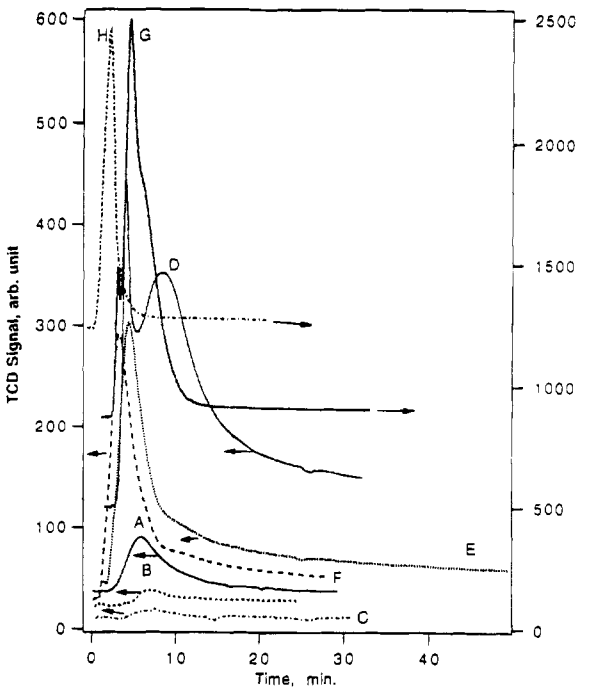

Figure 3. Monitored isothermal reduction of Ni-OMS-2 in CO/He: (A) at 383 K, first cycle; (B) at 383 K, second cycle; (C) at 383 K, third cycle; (D) at 493 K, first cycle; (E) at 493 K, second cycle; (F) at 493 K, third cycle; (G) at 583 K, first cycle; (H) at 583 K, second cycle.

with the temperature-ramping profile. Soaking temperatures of reduction of 383, 498, 573, 663, 793, and 943 K were determined from constant-ramping TPR data for Ni-OMS-2,[12] as shown in trace A in Figure 1. Compared to the unresolved triplet peak from 430 to 720 K in the constant-ramping TPR spectrum of Figure 1, trace A, the stepwise ramping TPR spectrum of Figure 1, trace B shows a considerable improvement in the resolution of the adjoined peaks. Stepwise-ramping TPR and constant-ramping TPR data in CO/He of Cu-OMS-2 are shown in Figure 2, trace C and Figure 2, traces A and B, respectively. The temperatures selected for stepwise TPR, based on the information provided from constant-ramping TPR, are 363, 463, 523, 563, 773, and 943 K. Six peaks appear in the stepwise-ramping TPR spectrum (Figure 2, trace C). Some of the peak maxima emerge during temperature ramping from one step to the next higher step, while others emerge just after the start of soaking. The CO consumption almost reaches the base line in each soaking period. Stepwise-ramping TPR spectra demonstrate a remarkable improvement of the demarcation of various oxygen species, which approaches a nearly complete resolution. Trace B of Figure 2 shows that the effect of considerably lowering the ramping rate (from 15 to 5 K/min) does not result in any improvement in the resolution of such oxygen species, as suggested in ref 15.

Monitored Isothermal Reduction and Reoxidation. The monitored isothermal reduction of Ni-OMS-2 was conducted at 383, 493, and 583 K. The results are shown in Figure 3. It is apparent that the reduction profiles become larger with increasing reduction temperature. Several cycles of reduction and reoxidation at each temperature were conducted. At one specified temperature, the reduction profiles diminish in subsequent cycles. Samples after each monitored isothermal reduction at 493 and 583 K were subjected to 16−30 oxygen pulses at respective reduction temperatures. Oxygen uptakes

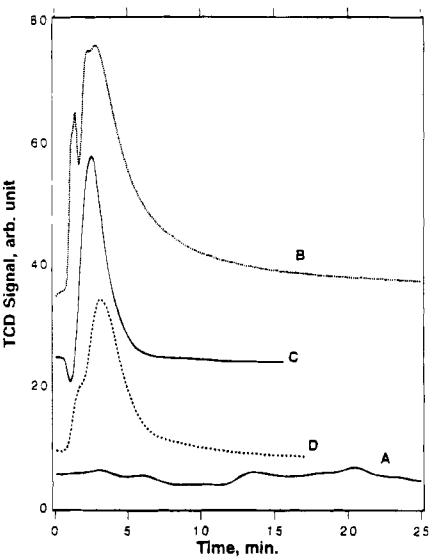

Figure 4. Monitored isothermal oxidation of reduced Ni-OMS-2 in O_2/He: (A) at 383 K, after 383 K first reduction; (B) at 673 K, after 383 K first reduction and A; (C) at 493 K, after 493 K first reduction; (D) at 493 K, after 493 K second reduction.

were extensive for the first seven or eight pulses but then diminished quickly. Parallel runs of monitored isothermal oxidations were conducted for Ni-OMS-2 materials reduced at 383 and 493 K, i.e., Figure 4. The sample after the first 383 K reduction showed no oxygen uptake at 383 K with a 4.80% O_2/He stream. Significant oxygen uptake was observed when an oxidizing stream at 673 K was used, as is shown in Figure 4. Later it will be shown that more oxygen is taken up in monitored isothermal reoxidation than with pulse reoxidation procedures.

Results of several cycles of monitored isothermal reductions

(15) Jones, A.; McNicol, B. D. *Temperature-programmed Reduction for Solid Materials Characterization*; M. Dekker, Inc.: New York, 1986.

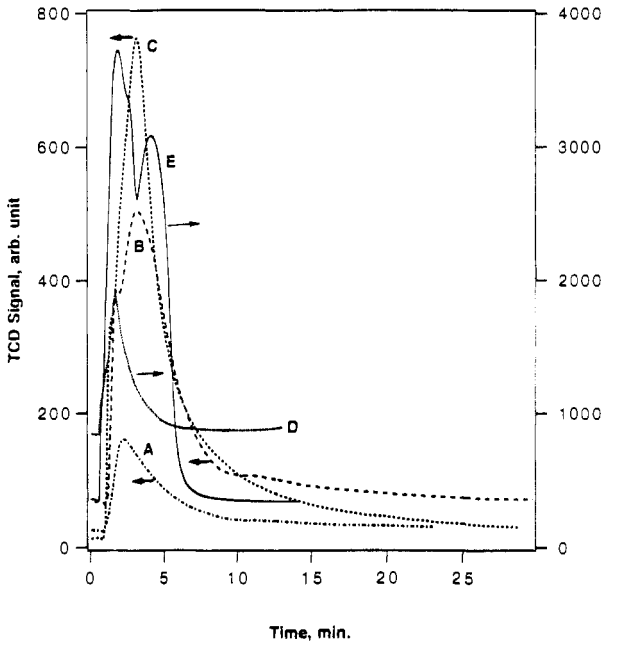

Figure 5. First cycle monitored isothermal reduction of Cu-OMS-2 in CO/He: (A) at 373 K; (B) at 463 K; (C) at 523 K; (D) at 563 K; (E) at 613 K.

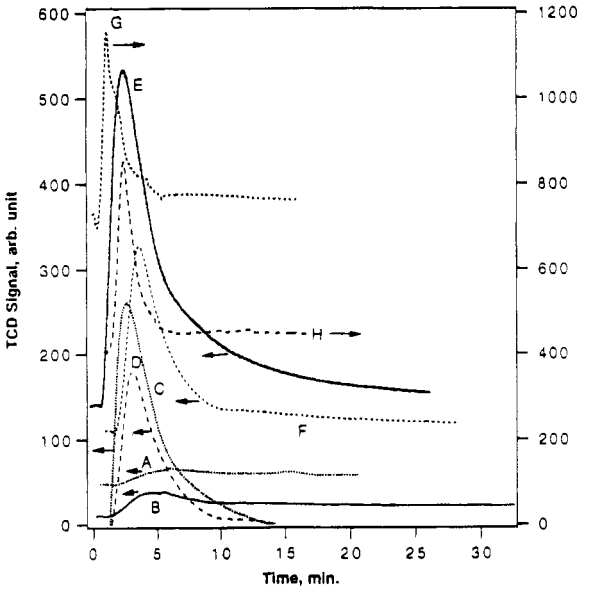

Figure 6. Subsequent cycle monitored isothermal reduction of Cu-OMS-2 in CO/He: (A) at 373 K, second cycle; (B) at 373 K, third cycle; (C) at 463 K, second cycle; (D) at 463 K, third cycle; (E) at 523 K, second cycle; (F) at 523 K, third cycle; (G) at 563 K, second cycle; (H) at 563 K, third cycle.

of Cu-OMS-2 at 373, 463, 523, 563, and 613 K are shown separately in Figure 5 (first cycle only) and Figure 6 (subsequent cycles). Again, qualitatively speaking, the areas under the reduction curves diminish with decreasing reduction temperature and increasing number of cycles. Reoxidation by oxygen pulsing of Cu-OMS-2 which previously was reduced at different temperatures and for various cycles are similar to those of Ni-OMS-2. Results of monitored isothermal oxidations in parallel runs for reduced samples are described in Figure 7. In both cases, oxygen recovery is diminished with decreasing temperature and increasing number of cycles.

X-ray Powder Diffraction. X-ray diffraction studies of several of the samples after reduction–reoxidation were conducted, and most of them show considerable decreases in intensity of hollandite/cryptomelane diffractions lines, see Figures 8 and 9.

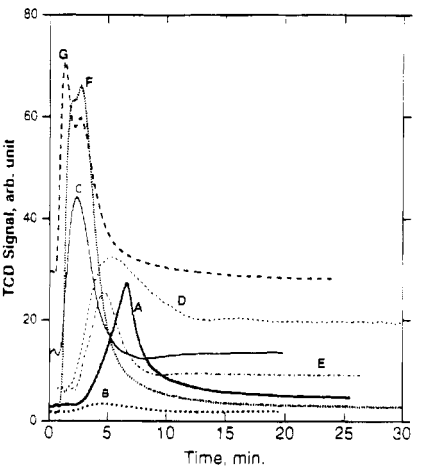

Figure 7. Monitored isothermal oxidation of reduced Cu-OMS-2 in O_2/He: (A) at 373 K, after 373 K first reduction; (B) at 373 K, after 373 K second reduction; (C) at 463 K, after first cycle reduction; (D) at 463 K, after second cycle reduction; (E) at 463 K, after fourth cycle reduction; (F) at 523 K, after first cycle reduction; (G) at 523 K, after second cycle reduction.

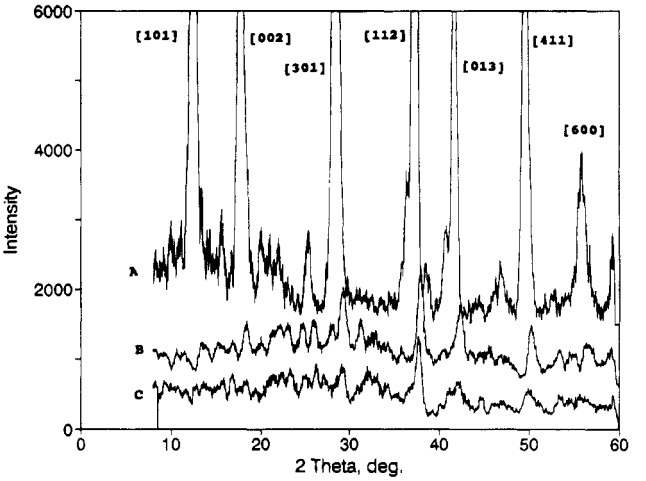

Figure 8. X-ray diffraction patterns of Ni-OMS-2 before and after redox cycles: (A) fresh sample; (B) after three 383 K redox cycles; (C) after three 493 K redox cycles.

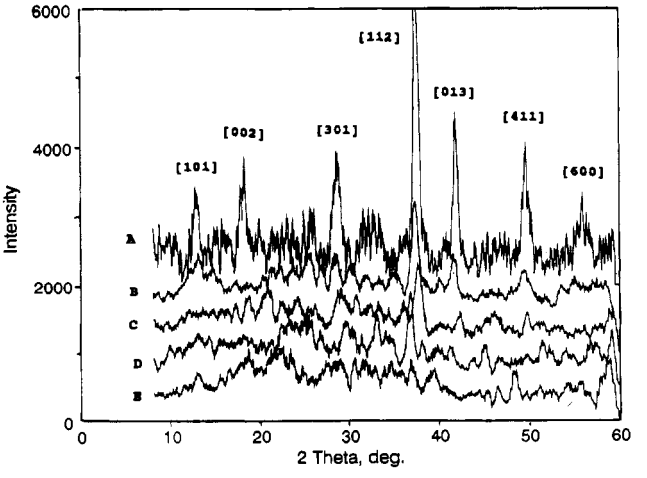

Figure 9. X-ray diffraction patterns of Cu-OMS-2 before and after redox cycles: (a) fresh sample; (B) after three 373 K redox cycles; (C) after three 463 K redox cycles; (D) after three 523 K redox cycles; (E) after one 613 K redox cycle.

Discussion

Comparison of Constant- and Stepwise-Ramping TPR Data. Theoretically speaking, among the three modes of reduction, the constant-ramping or conventional temperature-programmed mode, the stepwise-ramping temperature-programmed mode, and the monitored isothermal mode, the latter should be the most precise one for determining the availability of oxygen species reactive to carbon monoxide at a specific temperature. Apparently, this is because the reduction is strictly limited to a definite temperature. Thus, as the temperature of reduction does not go beyond a certain value, the oxygen species that are reactive at higher temperatures should remain inactive. Meanwhile, constant-ramping TPR methods lead to TPR peaks that are usually broad and sometimes overlapped, so the estimation of a particular oxygen species for a specific TPR peak cannot be considered to be precise. All oxygen species are exhausted in a single TPR run. The probed sample is usually transformed to other structures in an exhaustive reduction, as is the case for OMS materials of different structures.[11-13] Some oxygen species that are reactive only at higher temperatures are irreversibly depleted and cannot be recovered.

In the case of monitored isothermal reduction, information can be obtained about recoverability of oxygen species and restorability and even stability of some structures up to a certain threshold temperature. However, the temperatures to be selected for stepwise-ramping TPR or monitored isothermal reduction need to be determined from conventional TPR prior to stepwise-ramping and monitored isothermal experiments. It seems apparent that constant-ramping TPR is still needed for a preliminary understanding of the distribution of oxygen species in simple or mixed oxide materials. For more precise knowledge, constant-ramping methods are not sufficient and stepwise-ramping techniques or monitored isothermal reduction must be used if the resolution of the TPR peaks is poor. Since the constant-ramping TPR profiles of Cu-OMS-2 between 273 and 600 K (traces A and B in Figure 2) are structureless, the choice of a six-step ramp (as depicted in traces C and D in Figure 2) might not be unique. Although a detailed study of stepwise-ramping TPR is beyond the scope of this paper, an eight-step ramping procedure, with changes in soaking temperatures and some soaking times, was tried. Results show a pattern quite similar to trace C in Figure 2, with splitting of the 563 K peak into 533 and 573 K peaks of equivalent total peak area. Various ramping procedures do not generally affect our results or our ability to find regions where OMS-2 is stable or regenerable after redox processes.

The oxygen species consumed during reduction with CO/He which are related to the peaks in the TPR/CO spectra of Ni-OMS-2 and Cu-OMS-2 can be quantified by calibration, as described in ref 11. Similar procedures have been done for the stepwise reduction and monitored isothermal reduction, and the amounts of oxygen consumption at each specific temperature for the three modes of reduction are compared in Table 1 for Ni-OMS-2 and Cu-OMS-2, respectively. Note that, for monitored isothermal reduction, values for the first reduction cycle are used for comparison. Obviously, the amounts of oxygen species determined for each specific temperature for the two doped OMS-2 samples are quite close to each other for the monitored isothermal reduction and stepwise-ramping TPR. However, the amounts of oxygen species consumed during constant-ramping TPR are significantly larger than for the other two modes for all temperatures, except for the lowest temperature of reduction. This is probably due to the rapid rise in temperature and overlapping of part of the adjacent peaks in the constant-ramping mode.

Table 1. Oxygen Availability in Ni-OMS-2 and Cu-OMS-2 to Three Modes of Reduction by CO/He (in Percent of Lattice Oxygen)

	A. Ni-OMS-2				
reduction temp, K	383	493	583	680	
constant-ramping TPR	1	15	35	40	
stepwise-ramping TPR	1	10	20	30	
monitored isot redn	1	9	21		
	B. Cu-OMS-2				
reduction temp, K	373	463	523	563	613
constant-ramping TPR	2	10	17	24	35
stepwise-ramping TPR	2	8	14	17	24
monitored isot redn	2	6	11	15	28

Monitored Isothermal Methods. The isothermal technique should be able to be used to yield kinetic information concerning reduction and oxidation of OMS-2, as kinetic information had been drawn from studies on manganite perovskites.[8,16-18] Such kinetic analyses will be discussed elsewhere because the monitored isothermal reduction/oxidation profiles are rather complex and beyond the scope of the present discussion. Reduction of the two fresh OMS-2 samples at high temperatures (notably Si-OMS-2 at 493 and 583 K and Cu-OMS-2 at 613 K) proceeds in two consecutive stages; for example, refer to traces D and G of Figure 3 and trace E of Figure 5. Such consecutive stages even appear during monitored isothermal oxidation (see traces B and D in Figure 4 and traces D, F, and G in Figure 7) but do not generally happen during the later redox cycles.

The possibility of formation of a microcrystalline or even amorphous phase during the initial phase of reduction that covers the remaining crystalline phase and thus imposes diffusional resistance to the reduction process may explain the temporary decreases in the reduction rate. However, this cannot explain the existence of stagewise reoxidation phenomena and disappearance of such stagewise behavior during subsequent redox cycles. This behavior may be accounted for by a dynamic transition of oxygen species during the redox process. For example, some defects may be formed which induce transformation of nearby less reactive oxygen species (possibly oxygen in the Mn(II)−O−Mn(IV) bridge) to become reactive along with the depletion of certain oxygen species reactive at the specific temperature. Similar transformation of some anion vacancies nearby a newly filled oxygen anion could also explain the stagewise reoxidation. Such transformations, however, will not occur in the subsequent redox cycles, as the local structure becomes "annealed". Some of the reduction processes during subsequent redox cycles occur for a very long period, with the TCD signal returning very slowly to the base line. This also implies the existence of a slow transformation of less reactive oxygen species to more reactive ones.

The oxygen pulse data do not appear to provide kinetic information concerning reoxidation. This is because the oxygen uptake in the first few pulses is close to complete consumption; therefore, the supply of oxygen dominates the process.

Oxygen Recovery: Quantitative Aspects. The amounts of oxygen species depleted during reduction and recovered during reoxidation by oxygen pulsing and monitored isothermal oxidation have been calculated for different redox cycles at various temperatures. The results of these calculations are shown in Table 2 for Ni-OMS-2 and Cu-OMS-2. Reproducibility of

(16) Fierro, J. L. G.; Peña, M. A.; Tejuca, L. G. *J. Mater. Sci.* **1988**, *23*, 1018−1023.
(17) Tascón, J. M. D.; Oliván, A. M. O.; Tejuca, L. G.; Bell, A. T. *J. Phys. Chem.* **1986**, *90*, 791−795.
(18) Tascón, J. M. D.; Fierro, J. L. G.; Tejuca, L. G. *J. Chem. Soc., Faraday Trans. I* **1985**, *81*, 2399−2407.

Table 2. Oxygen Availability during Reduction and Uptake during Reoxidation (in Percent of Lattice Oxygen)

A. Ni-OMS-2

	temp, K							
	383			493			583	
no. cycle	1	5	6	1	2	3	1	2
monitored redn	1	<1	<1	9	4	4	21	8
oxygen pulsing				4	4	4	8	5
monitored oxidn	<1			18	10		6	

B. Cu-OMS-2

	temp, K										
	373			463			523			563	
no. cycle	1	2	3	1	2	3	1	2	3	1	2
monitored redn	2	1	1	6	3	3	11	7	5	15	6
oxygen pulsing	<1		<1	2	2	2	8	6	5	13	
monitored oxidn		1	<1	18	7		22			*a*	

[a] Cu-OMS-2 after 2nd reduction at 563 K wsa reoxidized in a continuous oxygen stream for 0.5 h.

parallel runs, as determined via multiple runs, is generally within 7.7−8.8%.

It is obvious that the oxygen removed from Ni-OMS-2 at 383 K is minuscule, only a little more than 0.2 atom/molecule (or 1.4% of the lattice oxygen). Oxygen recovered by monitored isothermal oxidation at 383 K is also nil, even for such a slight extent of oxygen depletion. Only data for monitored isothermal oxidation at 573 K show a modest recovery of 0.02 atom/molecule. Subsequent reductions in the second and third redox cycles show that nearly no recoverability of oxygen at this temperature can be achieved.

At 493 K, Ni-OMS-2 provides about 9% of its lattice oxygen (1.5 atom/molecule) reactive to CO reduction, and 38% of the depleted oxygen can be recovered after the first redox cycle. In the second and third redox cycles, both the oxygen depleted during reduction and that recovered during oxygen pulsing amounts to 3−4% of the lattice oxygen (0.6−0.7 atom/molecule), close to the amount of oxygen recovered in the first redox cycle.

The depletion of oxygen atoms from Ni-OMS-2 at 583 K is more than doubled, 21% of the lattice oxygen, than for reduction at 493 K. The recovery of oxygen from the first reduction is also doubled (8% of the lattice oxygen) for the 583 K cycle. The recovery of oxygen from the second reduction cycle, however, is only slightly greater than that of the corresponding 493 K cycle.

The availability of oxygen to CO oxidation in the first cycle for Cu-OMS-2 at low temperature (373 K) amounts to 2% of the lattice oxygen and is considerably greater than Ni-OMS-2 (at 383 K). Although the recovery by oxygen pulsing for the freshly reduced Cu-OMS-2 is very poor (even less than 0.01 atom/molecule), the availability of oxygen for CO oxidation in the second redox cycle still amounts to about 0.5% of the lattice oxygen. However, if monitored isothermal oxidation with 4.80% O_2/He is applied during the second redox cycle, much higher oxygen recovery (about 1.3% of the lattice oxygen) was observed, as indicated and explained in the Regeneration of OMS-2 Materials section. Oxygen depleted in the third redox cycle can reach 0.8% of the lattice oxygen. Oxygen recovery in the third redox cycle by oxygen pulsing, however, is even less than that in the first redox cycle, only half of that amount.

The three redox cycles of Cu-OMS-2 at 463, 523, and 563 K display similar trends of increasing available oxygen for reduction and oxygen recovery, which is always significantly lower than the former. The extent of oxygen recovery increases, from approximately 2% at 373 K to 40−60% at 463 K, approximately 75% at 523 K, and approximately 85% at 563 K. The extent of oxygen recovery via oxygen pulsing for Ni-OMS-2, on the other hand, remains at less than 40% for the 493 and 583 K runs.

Structural Considerations. The retention of the hollandite/cryptomelane structure for the treated samples can be judged from the X-ray diffraction patterns. It is apparent that almost all of the diffraction peaks of hollandite/cryptomelane diminish in intensity to different extents, as shown by the X-ray diffraction patterns of fresh Cu-OMS-2 and those after redox cycles at 373, 463, 523, and 613 K in Figure 9. However, samples subjected to redox cycles at 373 and 463 K still retain most of the diffraction peaks of cryptomelane/hollandite, notably the [112] peak at 2.391 Å and the [301], [013], and [411] peaks at 3.124, 2.156, and 1.842 Å, respectively. It is also apparent that a considerable fraction of the sample clearly loses some long-range order. From X-ray diffraction peak broadening, it was calculated that, for Cu-OMS-2 after redox cycles at 373 and 463 K, the crystallite sizes diminish from 17.2−17.7 nm (from [112] and [013] reflections) to 10.9−11.6 and 8.3−8.8 nm, respectively. For Ni-OMS-2 after redox cycles at 383 and 493 K, the crystallite sizes diminish from 9.0−16.5 nm (from [013] and [112] peaks) to 6.2−13.5 and 3.6−5.5 nm, respectively.

As suggested by a reviewer, our XRD data suggest that an amorphous phase could be formed after the redox cycles, and the remainder of cryptomelane material could be covered by this amorphous phase and protected from further collapse of the crystalline material by diffusional constraints. Since the monitored isothermal reduction/oxidation proceeded for a sufficiently long time after the return of the TCD signal to the base line, it is conceivable that the amorphous material may not prevent diffusion of CO or oxygen into the interior of crystallites.

For samples treated at 523 K, the only identifiable [112] peak undergoes some shift in position to a lower diffraction angle. At 613 K, no more cryptomelane/hollandite diffraction peaks are observed. Regarding the recoverability of oxygen into reduced Cu-OMS-2, it is obvious that 463 K should be the most preferable temperature for redox reactions of Cu-OMS-2, which is high enough to assure the greatest recoverability of oxygen (40−60%) without causing extensive collapse of the hollandite/cryptomelane structure, as shown in Figure 9.

Figure 8 shows the X-ray diffraction patterns for fresh Ni-OMS-2 and after redox cycles. In addition to a similar diminution in diffraction intensities for samples treated at 383 and 493 K, the pronounced [112], [013], and [301] diffraction peaks of the hollandite/cryptomelane structure are all shifted slightly to smaller d spacings. Such shifts in diffraction peaks can be accounted for by the presence of defects formed due to oxygen anion removal during reduction, as suggested by Soderholm *et al.*[19] Consequently, excessive formation of defects culminates in a decrease of long-range order to an amorphous state.

It seems evident that the Ni-OMS-2 structure is not as stable as that of Cu-OMS-2. As mentioned above, copper ion can have a much higher extent of exchange of potassium ion than nickel ion at the same concentration. Additional TP results show that K-OMS-2 is even more unstable in redox cycles. The higher stability of Cu-OMS-2 implies a stabilizing action of copper.

(19) Soderholm, L.; Morss, L. R.; Mohar, M. F. *J. Less-Common Met.* **1987**, *127*, 131−135.

The crystallographic behavior of normal oxides of transition metals following partial removal of lattice oxygen falls into three categories. For the first category, it is established that the formation of WO_{3-x}, NbO_{3-x}, and TiO_{2-x} from partial reduction of tungsta, niobia, and titania involves collapse and crystallographic shear. For the second category, partial reduction of manganite perovskite ($CaMnO_3$) up to removal of $^1/_6$ of the total lattice oxygen leads to formation of $CaMnO_{2.5}$, which results in minor structural reorganization, with retention of the essential features of the fully oxidized precursor $CaMnO_3$.[20] The reduced sample was claimed to be easily reoxidized by air oxidation at 573 K, with full restoration of the original structure. $CaMnO_3$ is a perovskite-related oxide, with Mn in its quadrivalent state, and is composed of corner-linked MnO_6 octahedra. The Mn(III) ions formed by reduction were found in square-pyramidal coordination with oxygen.[21-23] The perovskite $La(Mn,Cu)O_3$ also showed a structural stability limit to $ABO_{2.5}$.[24] The cryptomelane/hollandite structure related to that of OMS-2 (composed mainly of edge-linked MnO_6 octahedra)[25] seems to belong to a third category that does not possess the same structural stability as $CaMnO_3$. The oxygen depletion from Cu-OMS-2 at 463 K is less than $^1/_{16}$ of the total lattice oxygen, and some structural restoration is possible, depending on reaction conditions.

Regeneration of OMS-2 Materials. Parallel reoxidation data usually show more oxygen recovery by means of monitored isothermal oxidation than by oxygen pulsing, as shown in Table 2. In addition, some samples after reduction by CO/He have been submitted to double re-oxidation, first by oxygen pulsing, followed by monitored isothermal oxidation. The oxygen recovery from 583 K reduced Ni-OMS-2 by oxygen pulsing is about 1.3 atom/molecule. More oxygen (about 1.0 atom/molecule) is taken up during subsequent monitored isothermal oxidation. While the oxygen recovery of Cu-OMS-2 reduced at 373 K via oxygen pulsing is only 0.004 atom/molecule, further oxygen recovery of 0.04 atom/molecule is achieved with a succeeding monitored isothermal reduction at the same temperature.

However, oxygen depletion of the doubly reoxidized Ni-OMS-2 in the second 583 K redox cycle is still only 1.3 atom/molecule, the same as the amount of oxygen uptake during oxygen pulsing. For Cu-OMS-2, the reactive oxygen available to the second monitored isothermal reduction, after a previous oxygen pulsing, at 373 K is 0.09 atom/molecule, while that available to the third reduction, after a second monitored isothermal oxidation, amounts to 0.12 atom/molecule, again close to each other.

In one respect, these experiments clearly show that oxygen uptake depends strongly on the severity of re-oxidation. In oxygen pulsing, oxygen partial pressure present during reoxidation could be low due to dilution by a large volume of helium carrier gas. The pulsing period is rather short. Moreover, the sample under reoxidation treatment was repeatedly subjected to helium purging after the oxygen pulses passed. Meanwhile, the monitored isothermal oxidation was carried out at possibly higher oxygen pressure in a much longer period, usually 30–40 min till the return of the TCD signal base line for a substantially long time. In another respect, the excess oxygen uptake during monitored isothermal oxidation over oxygen pulsing does not contribute to more reactive oxygen available during subsequent reduction. This might be explained by considering that the excess oxygen is in some form of chemisorbed oxygen. In relation to the TPD and TPR (either in hydrogen or in carbon monoxide) studies,[12] the oxygen species corresponding to the medium- and high-temperature peaks in TPD and TPR are lattice oxygen coordinated to the Mn ions, while those corresponding to low-temperature peaks in TPD are more likely due to chemisorbed oxygen. The monitored isothermal data presented here give further support for this hypothesis. Such chemisorbed oxygen will not participate in the subsequent reduction by CO, since it is desorbed during He purging immediately following the monitored isothermal oxidation in order to prepare the sample for the next reduction.

Conclusions

The following conclusions were reached in studies reported here. (1) Stepwise-ramping TPR obviously gives much better resolution of adjoined peaks than constant-ramping TPR. (2) With preliminary knowledge gained from TPR (either constant or stepwise-ramping), monitored isothermal reduction techniques offer a convenient approach for obtaining knowledge about the availability of reactive oxygen in mixed metal oxides and its recoverability, in addition to the restorability of relevant crystallographic structures of the oxides. Monitored isothermal techniques provide data that suggest that reductions and oxidations at specific temperatures can proceed in two stages. (3) Oxygen in Cu-OMS-2 and Ni-OMS-2 can be reversibly removed by reduction with CO and recovered by re-oxidation for several redox cycles. Oxygen removal increases with higher reduction temperature. Higher re-oxidation temperature favors a higher extent of oxygen recovery. The oxygen recovery is significantly higher for Cu-OMS-2 than for Ni-OMS-2. (4) The cryptomelane/hollandite structure of Cu-OMS-2 can be retained to a significant extent after several redox cycles at lower temperatures. The retention of the OMS-2 structure seems better for Cu-OMS-2 than Ni-OMS-2. Structural collapse becomes severe at higher redox temperatures. (5) Optimum oxygen recovery and structure retention can be achieved at 463 K for Cu-OMS-2 redox treatment.

Acknowledgment. We acknowledge the Department of Energy, Office of Basic Energy Sciences, Division of Chemical Sciences, and Texaco, Inc., for support of this research.

IC940953W

(20) Reller, A.; Jefferson, D. A.; Thomas, J. M.; Uppal, M. K. *J. Phys. Chem.* **1983**, *87*, 913–914.
(21) Chiang, C. C. K.; Poeppelmeier, K. R. *Mater. Lett.* **1991**, *12* (1/2), 102–108.
(22) Reller, A.; Jefferson, D. A.; Thomas, J. M.; Beyerlein, R. A.; Poeppelmeier, K. R. *J. Chem. Soc., Chem. Commun.* **1982**, 1378–1380.
(23) Poeppelmeier, K. R.; Leonowicz, M. F.; Longo, J. M. *J. Solid State Chem.* **1982**, *44*, 89–98.
(24) Chan, K. S.; Ma, J.; Jaenicke, S.; Chuah, G. K. *Appl. Catal. A.* **1994**, *107*, 201–227.
(25) Byström, A.; Byström, A. M. *Acta Crystallogr.* **1950**, *3*, 146–154.